INTERNATIONAL JOURNAL FOR NUMERICAL METHODS IN FLUIDS
Int. J. Numer. Meth. Fluids 2003; **43**:115–127 (DOI: 10.1002/fld.588)

A vertically moving grid finite-element modelling of tidal flow in the Changjiang Estuary, China

Z. Shi[1,*,†], S. S. Li[2] and O. S. Petersen[3]

[1] *Department of Harbour & Coastal Engineering, School of Naval Architecture & Ocean Engineering, Shanghai Jiao Tong University, 1954 Hua Shan Road, Shanghai 200030, China*
[2] *Department of Harbour Engineering, School of Civil Engineering, Tianjin University, 92 Weijin Road, Tianjin 300072, China*
[3] *DHI Water & Environment-Agern Alle 11, DK-2970 Horsholm, Denmark*

SUMMARY

An estuarine two-dimensional vertical finite-element model of tidal flow has been established by laterally integrating Navier–Stokes equation. To this end, a moving grid finite-element method has been used. An arbitrarily shaped quadrilateral element has been selected. This model has been validated by using field data from two monitoring stations at the North Passage of the Changjiang Estuary. Using this numerical model, two types of modelled results were obtained: (1) vertical distributions of tidal current velocities at the North Passage of the Changjiang Estuary; (2) longitudinal distributions of tidal current velocities at maximum flood tide, at high slack water, at maximum ebb tide and at low slack water tide at the North Passage of the Changjiang Estuary. The conclusion is that the model provides a reasonable agreement with observed data. Copyright © 2003 John Wiley & Sons, Ltd.

KEY WORDS: moving grid; finite element; tidal flow; the Changjiang Estuary

1. INTRODUCTION

Tidal flow is the main hydrodynamic force in estuaries. Both scientists and engineers have been interested in tidal flow because of its significance in estuarine hydraulics, harbour construction, channel dredging and pollutant monitoring. To this end, numerical models have been developed that provide an effective method to simulate estuarine flows. Two principal types of two-dimensional (2D) numerical models have been used, i.e. two-dimensional horizontal (2DH) [1–4] and two-dimensional vertical (2DV) models [4–8]. 2DH models, based on the

*Correspondence to: Zhong Shi, Department of Harbour & Coastal Engineering, School of Naval Architecture & Ocean Engineering, Shanghai Jiao Tong University, 1954 Hua Shan Road, 200030 Shanghai, People's Republic of China.
† E-mail: zshi@sjtu.edu.cn

Contract/grant sponsors: National Science Fund for Distinguished Young Scholars of China; contract/grant number: Estuarine and Coastal Studies 40225014; and Shanghai Rising-Star Program

Received 17 April 2002
Revised 21 April 2003

depth-integrated equations, could simulate the horizontal distributions of tidal flows, but vertical variations are parameterized or treated in terms of analytic functions. 2DV models, based on the width-integrated equations are well-suited to predict the vertical distributions of tidal flow in narrow estuaries. Numerical methods comprise finite-difference methods (FDM) and finite-element methods (FEM) have been commonly used (e.g. FDM [7–10]; FEM [11–21]).

In 2DH models, where the vertical discretization is important, a σ-co-ordinate transformation, combined with FDM has also been used to resolve significant variations in estuarine bottom topography and tidal elevations [6, 22–24]. Using a σ-co-ordinate transformation the computing domain is resolved by a constant number of sub-layers, enabling the computation in the σ-direction to be performed on a fixed grid.

FEM, based on variational principles or weighted residual method [25], is a general approach to solve partial differential equations, appropriate when dealing with estuarine complex bathymetry and land boundaries. According to whether the computing area and grid are varying or not, it can be grouped into three types: (1) traditional FEM with any fixed computing area and grid; (2) auto-adaptive FEM with a fixed computing area and varying grids; and (3) moving grid FEM with varying computing areas and grids. In 2DV numerical models of estuarine tidal flow, computing areas and grids must vary with the tidal elevation. In this paper, an FEM method where a σ-co-ordinate transformation is not necessary when using vertically moving grids will be derived.

The primary objective of the present paper is to develop and verify a 2DV estuarine tidal model derived by the moving grid FEM, coupled with a turbulence closure sub-model. The present model was developed by Li and Shi [26]. This represents a first step towards developing a general 2DV estuarine model.

2. NUMERICAL MODEL

2.1. Governing equations

Considering a right-hand Cartesian co-ordinate system (Figure 1), the governing equations can be obtained by integrating Navier–Stokes equations over estuarine width (y direction, Figure 2). The following assumptions are made: (1) hydrostatic approximation of the vertical momentum equation; (2) ignoring lateral variations of the momentum distributions; (3) the Coriolis acceleration is omitted; (4) Boussinesq approximation; and (5) the non-slip conditions

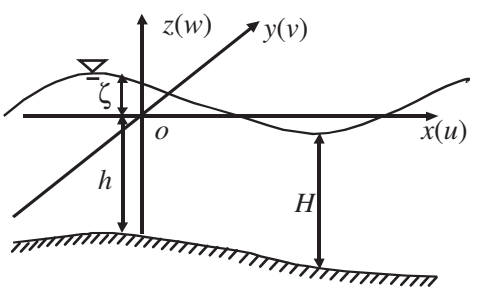

Figure 1. Cartesian co-ordinate system.

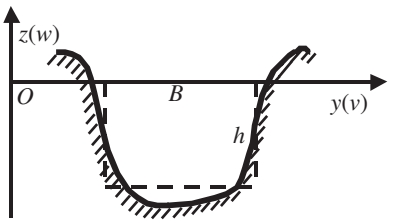

Figure 2. Schematic estuarine cross-section.

on the two sides of the estuary (where $u = v = w = 0$). Then we can obtain the width-averaged equations for conservation of estuarine tidal water mass and momentum:

Continuity equation

$$\frac{\partial Bu}{\partial x} + \frac{\partial Bw}{\partial z} = 0 \tag{1}$$

Tidal elevation equation

$$\frac{\partial \varsigma}{\partial t} + \frac{1}{B}\frac{\partial}{\partial x}\left(B\int_{-h}^{\varsigma} u\,\mathrm{d}z\right) = 0 \tag{2}$$

Momentum equation

$$\frac{\partial Bu}{\partial t} + u\frac{\partial Bu}{\partial x} + w\frac{\partial Bu}{\partial z} + \frac{B}{\rho}\frac{\partial p}{\partial x} = \frac{\partial}{\partial x}\left(B\varepsilon_x\frac{\partial u}{\partial x}\right) + \frac{\partial}{\partial z}\left(B\varepsilon_z\frac{\partial u}{\partial z}\right) \tag{3}$$

Hydraulic pressure

$$p = p_a + \rho g(\varsigma - z) \tag{4}$$

where t denotes time; ς the tidal elevation above the mean water level; ε_x and ε_z components of eddy viscosities in x and z directions; p pressure; p_a intensity of pressure; ρ the fluid density; g the gravity acceleration; u and w components of tidal flow velocities in x and z directions; $B = B(z)$ the estuarine width (a function of depth); h the estuarine depth (Figure 2); $H = \varsigma + h$ the total water depth; and x and z horizontal and vertical Cartesian co-ordinates.

Lateral dispersion is very important in the modelling of tidal flow in estuaries. The consequences of neglecting the very important lateral dispersion would be to overestimate or underestimate the tidal flow. However, for the narrow and deep channel in estuaries (e.g. the North Passage of the Changjiang Estuary), lateral dispersion is not too important and can be neglected while vertical dispersion is important.

2.2. Boundary and initial conditions

(a) *Open boundaries*: Tidal elevation and velocity in each vertical layer can be specified at the open boundaries. Boundary conditions of tidal elevation and velocities should be given. However, the open boundary for tidal velocities in each vertical layer cannot be given in many cases. According to St Venant's principle, the influence will be limited to the nearby open boundary.

(b) *At the bottom*:

$$\rho\varepsilon_z\left(\frac{\partial u}{\partial z}\right)_{z=-h} = \tau_b \quad (\tau_b \text{ is the bottom friction shear stress}) \tag{5}$$

where τ_b can be related to the lowest node by means of a friction law.

(c) *At the free water surface*:

$$\rho\varepsilon_z\left(\frac{\partial u}{\partial z}\right)_{z=\varsigma} = \tau_w \quad (\tau_w \text{ is the surface wind shear stress}) \tag{6}$$

Initial values for both tidal elevation and velocity distribution must be specified. The former is obtained by linear interpolation between the upper and lower boundaries values, while the latter is taken as a logarithmic profile or a constant value: $\varsigma|_{t=0} = \varsigma_0, u|_{t=0} = u_0, w|_{t=0} = w_0$.

2.3. Eddy viscosities

The horizontal eddy viscosity is defined as [27]

$$\varepsilon_x = K_x H u \Delta t \left(1 - \frac{r}{R}\right)\sqrt{\left(\frac{\partial u}{\partial z}\right)^2 + \left(R\,\frac{\partial^2 u}{\partial z^2}\right)^2} \tag{7}$$

where $K_x = 5\sim10$; Δt is the time increment; R the average length of the main flow line; r the direct distance between the calculating point and the side of the estuary. This approach does not include lateral dispersion effects.

The vertical eddy viscosity is obtained from the Prandtl's mixing length assumption [27]

$$\varepsilon_z = K_1 l_m^2 \left|\frac{\partial u}{\partial z}\right| f(R_i) \tag{8}$$

where $R_i = -g(\partial\rho/\partial z)/\rho(\partial u/\partial z)^2$ is the Richardson number, accounting for the effect of vertical density gradients on the vertical momentum exchange; $f(R_i) = (1 + \beta R_i)$, $\beta = 1.0$; K_1 the coefficient; the mixing length

$$l_m = \begin{cases} K(z - z_0) & (0 \leqslant z \leqslant 0.3H) \\ K(0.3H - z_0) & (0.3H \leqslant z \leqslant H)' \end{cases}$$

where K is the von Karman's constant; $z_0 = K_s/30$ and K_s the roughness length.

3. MOVING GRID FEM DERIVATIONS

3.1. Derivations of the continuity and momentum equations

Derivations of the following equations are restricted within any local element (Figure 3). Considering an arbitrarily shaped quadrilateral element (Figure 3(a)), the isoparametric co-ordinate $[(\xi_n, \eta_n),\ (n = 1, 2, 3, 4)]$ (Figure 3(b)), ranging from 0 to ±1, is established at the centroid of

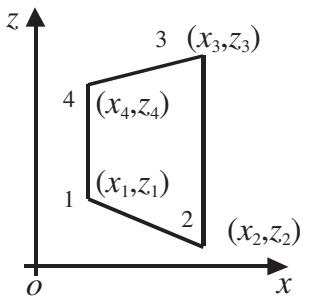

(a) Reference Cartesian co-ordinate

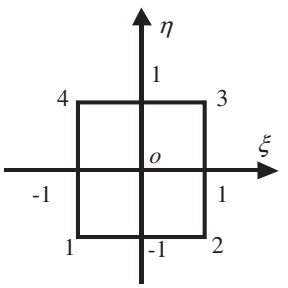

(b) Isoparametric co-ordinate

Figure 3. Four-node isoparametric element.

the element. The reference Cartesian co-ordinate $[(x_i, z_i),\ (i = 1,2,3,4)]$ (Figure 3(a)) is related to the isoparametric co-ordinate as $x = \sum x_i N_i,\ z = \sum z_i N_i$. Where N_i is the isoparametric function [28]:

$$N_n(\xi,\eta) = \tfrac{1}{4}(1 + \xi_n\xi)(1 + \eta_n\eta) \quad (n = 1,2,3,4)$$

Let $Bu = r, Bw = q$, and introduce a set of functions: $r = \sum r_i N_i,\ q = \sum q_i N_i,\ p = \sum p_i N_i$, $B = \sum B_i N_i$, in which r_i, q_i, p_i, B_i are the numerical values of variables at the element node points. Because these functions are approximate ones, if substituted into Equations (1) and (3), they will not exactly satisfy the governing differential equations and may result in an error or residual ε. Using the Galerkin weighted residual method, the inner product is set to zero $[(\varepsilon, N_j) = 0, (j = 1,2,3,4)]$ [25].

Thus, the local finite-element equations can be written as

$$AR + A_1 Q = 0 \tag{9}$$

(Note that $AR = \partial Bu/\partial x,\ A_1 Q = \partial Bw/\partial z$)

$$C\dot{R} + DR + ER + FP + GR + HR = 0 \tag{10}$$

(Note that $C\dot{R} = \partial Bu/\partial t$; advection matrix $DR = u\partial Bu/\partial x$; $ER = w\partial Bu/\partial z$; $FP = (B/\rho)\partial p/\partial x$; horizontal diffusion matrix $GR = -\partial/\partial x[B\varepsilon_x \partial u/\partial x]$; vertical diffusion matrix $HR =$

$-\partial/\partial z[B\varepsilon_z(\partial u/\partial z)]$) where

$$\dot{R} = \left(\frac{\partial r_1}{\partial t}, \frac{\partial r_2}{\partial t}, \frac{\partial r_3}{\partial t}, \frac{\partial r_4}{\partial t}\right)^{\mathrm{T}}; \quad R = (r_1, r_2, r_3, r_4)^{\mathrm{T}}; \quad P = (p_1, p_2, p_3, p_4)^{\mathrm{T}}$$

$$Q = (q_1, q_2, q_3, q_4)^{\mathrm{T}}$$

A, A_1, C, D, E, F, G representing matrices of the size 4×4 can be written as (the integration may be performed by means of the Gaussian quadrature): $a_{ij} = \iint_e \partial N_j/\partial x\, N_i |J|\, \mathrm{d}\xi\, \mathrm{d}\eta$

$$a_{1ij} = \iint_e \frac{\partial N_j}{\partial z} N_i |J|\, \mathrm{d}\xi\, \mathrm{d}\eta, \quad c_{ij} = \iint_e N_i N_j |J|\, \mathrm{d}\xi\, \mathrm{d}\eta$$

$$d_{ij} = \iint_e \frac{\partial N_j}{\partial x} N_i |J| \sum u_k N_k\, \mathrm{d}\xi\, \mathrm{d}\eta, \quad e_{ij} = \iint_e \frac{\partial N_j}{\partial z} N_i |J| \sum w_k N_k\, \mathrm{d}\xi\, \mathrm{d}\eta$$

$$f_{ij} = \frac{1}{\rho} \iint_e \frac{\partial N_j}{\partial x} N_i |J| \sum B_k N_k\, \mathrm{d}\xi\, \mathrm{d}\eta, \quad g_{ij} = \iint_e \varepsilon_x \frac{\partial N_i}{\partial x} \frac{\partial N_j}{\partial x} |J|\, \mathrm{d}\xi\, \mathrm{d}\eta$$

$$h_{ij} = \iint_e \varepsilon_z \frac{\partial N_i}{\partial z} \frac{\partial N_j}{\partial z} |J|\, \mathrm{d}\xi\, \mathrm{d}\eta, \quad J = \begin{vmatrix} \dfrac{\partial x}{\partial \xi} & \dfrac{\partial y}{\partial \xi} \\ \dfrac{\partial x}{\partial \eta} & \dfrac{\partial y}{\partial \eta} \end{vmatrix}$$

is Jacobian matrix: $|J|$ is the determinant of Jacobian J; and e is element index.

3.2. Derivation of the tidal elevation equation

Considering a one-dimensional element (two-node system) as shown in Figure 4, the shape functions have the forms [28]: $N_1 = \frac{1}{2}(1 - \xi)$, $N_2 = \frac{1}{2}(1 + \xi)$, in which, $\xi = (x - x_c)/l/2$, l is the length of the element, and x_c the reference Cartesian co-ordinate of the element centre (Figure 4).

Let $\int_{-h}^{\varsigma} u\, \mathrm{d}z = \alpha$ and introduce a set of functions in the form $B = \sum B_i N_i$, $\varsigma = \sum \varsigma_i N_i$, $\alpha = \sum \alpha_i N_i$. $B_i, \varsigma_i, \alpha_i$ are the numerical values of variables at the element node points. Because these functions are approximate ones too, if substituted into Equation (2), it may result in an error or residual ε. Using the Galerkin weighted residual method, the inner product is set to zero $[(\varepsilon, N_j) = 0, (j = 1, 2)]$ [28].

Thus, the local finite-element equation has the form

$$A_2 \dot{\varsigma} + B_1 \Delta + \frac{C_1}{B} \frac{\partial B}{\partial x} \Delta = 0 \tag{11}$$

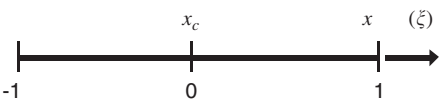

Figure 4. One-dimensional two-node element.

where

$$\dot{\varsigma} = \left(\frac{\partial \varsigma_1}{\partial t}, \frac{\partial \varsigma_2}{\partial t}\right)^{\mathrm{T}}; \quad \Delta = (\alpha_1, \alpha_2)^{\mathrm{T}}; \quad A_2 = \frac{l}{6}\begin{vmatrix} 2 & 1 \\ 1 & 2 \end{vmatrix}; \quad B_1 = \frac{1}{2}\begin{vmatrix} -1 & 1 \\ -1 & 1 \end{vmatrix}; \quad C_1 = \frac{l}{6}\begin{vmatrix} 2 & 1 \\ 1 & 2 \end{vmatrix}$$

For unsteady flow, the time derivative will be replaced by various forms of finite differences. In general, the explicit scheme is conditionally stable while the implicit scheme is unconditionally stable for any time increment and needs more computational resource due to non-linear matrix algebraic equations. Therefore, an explicit scheme, Euler scheme is used for time marching. This restricts the time step to Courant numbers, based on the gravity wave, below 1. However, any attempt to perform stability analysis is a formidable task and so the time increment is mostly acceptable throughout the numerical modelling.

Time discretization scheme is needed for unsteady flow. Generally, the differential implicit scheme is unconditionally stable, and allows a larger time increment. For time step, however, it is required to solve the non-linear algebra equations with a lot of calculations. Therefore, time discretization scheme with the finite-element method, the explicit scheme is conditionally stable. For two-dimensional finite-element equations, it is difficult to get stable justification using analytical method. Time step is actually determined using the numerical experimental method.

Local element coefficients are assembled using a Boolean matrix, which locates the appropriate local nodal contribution in the corresponding global system. Global finite-element equations have the same forms with the local ones. As shown in Figure 5(a), the computing areas, grids and the variables $[\varsigma_{n\Delta t}, u^a_{n\Delta t}, w^a_{n\Delta t}]$ at time $[n\Delta t]$ are all known. Tidal elevation $\varsigma_{(n+1)\Delta t}$ at time $[(n+1)\Delta t]$ can be obtained from Equations (11), (5) and (6). Due to the varying free surface, the computing areas and grids should be updated according to $\varsigma_{(n+1)\Delta t}$ (Figure 5(b)). Because of the varying areas and the grids, the velocity distributions $[u^b_{n\Delta t}$ or $w^b_{n\Delta t}]$ are obtained by linear interpolation in the velocity distributions $[u^a_{n\Delta t}$ or $w^a_{n\Delta t}]$. If the time increment Δt is small enough, this step can be omitted. Velocities $[u^b_{(n+1)\Delta t}]$ and $[w^b_{(n+1)\Delta t}]$ can be obtained from Equations (10) and (9). Then the same steps above will be repeated in the following cycle. The same topologies of two adjacent grids keep the section locations fixed, but the z co-ordinate changes.

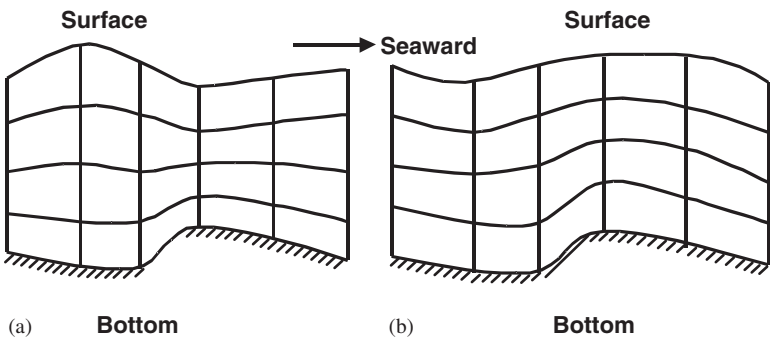

Figure 5. Meshes of two adjacent times: (a) Time $n\Delta t$; (b) Time $(n+1)\Delta t$.

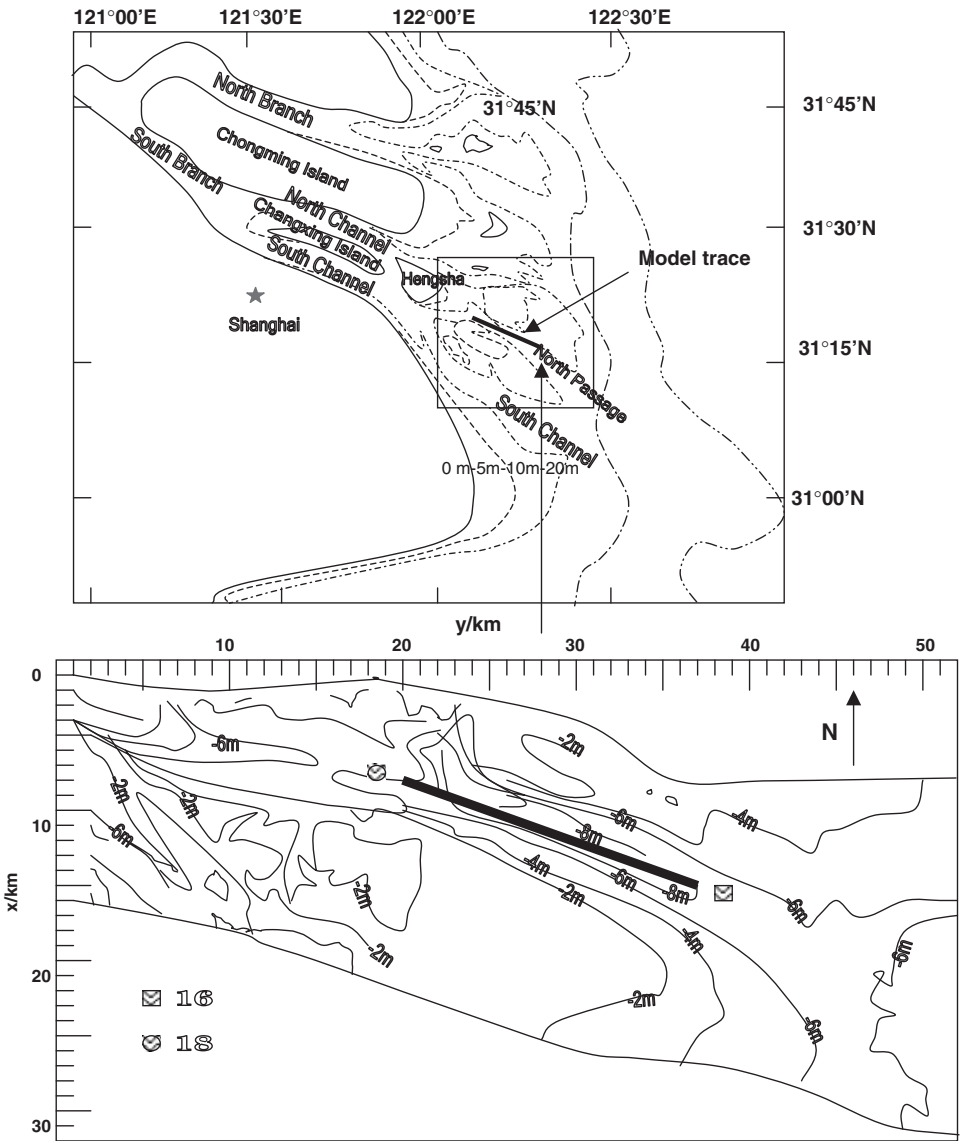

Figure 6. Contour map of the North Passage of the Changjiang Estuary and monitoring stations (a flat line on the map along the North Passage, showing where the model domain is).

4. APPLICATION OF MODEL TO THE CHANGJIANG ESTUARY

The Changjiang (Yangtze) is the fourth largest river in terms of both water and sediment discharge in the world. The mean annual river discharge is $2.9 \times 10^4\ m^3\ s^{-1}$. The Changjiang Estuary is a mesotidal estuary with a mean tidal range of 2.9 m. It consists of the North

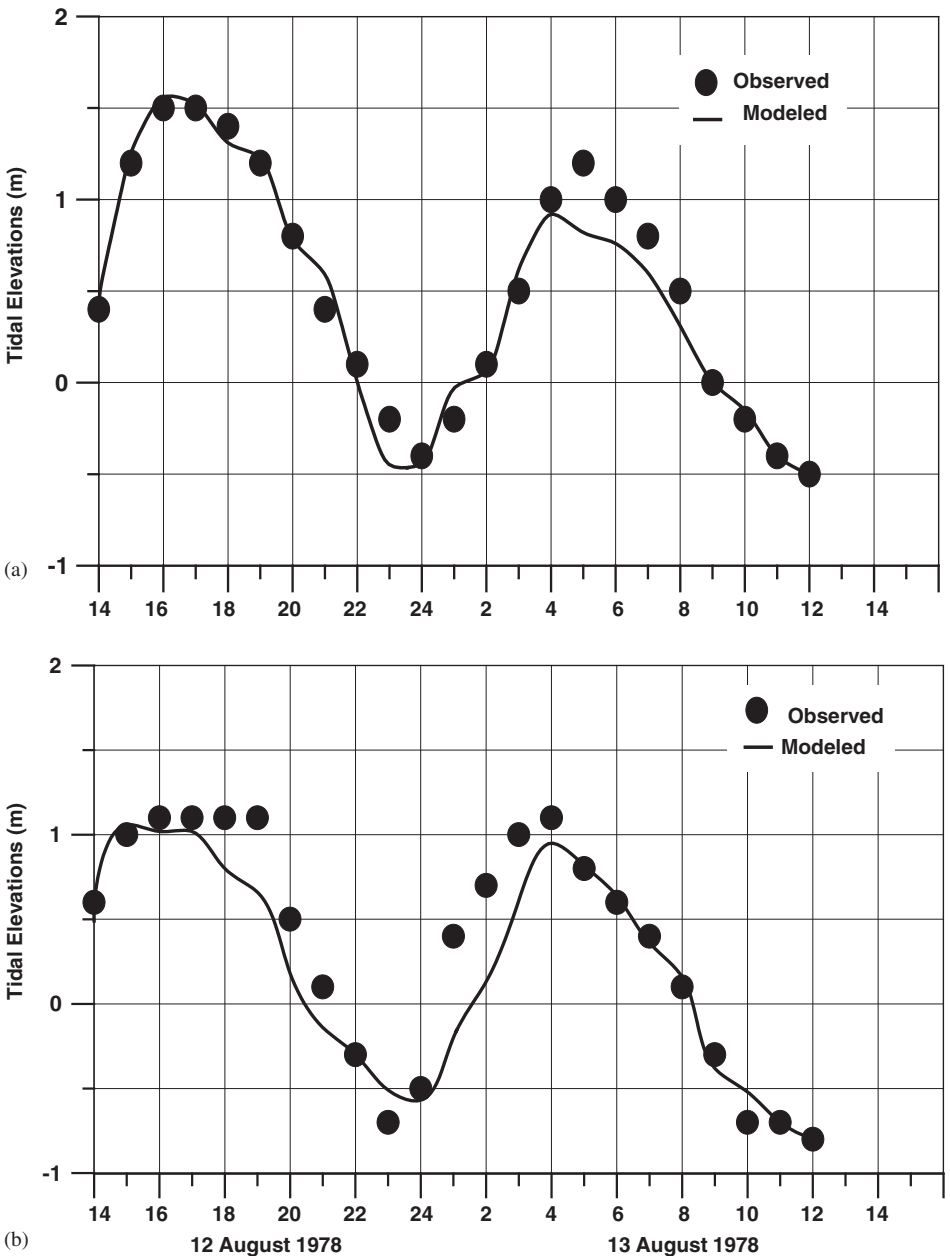

Figure 7. Comparisons of observed and modelled tidal elevations at Stations 16 and 18.

Branch, the South Branch, the North Channel, the South Channel, the North Passage and the South Passage (Figure 2). The North Passage has been chosen as a deep-water navigational channel (depth 7.5–10.0 m), and it is therefore regularly dredged. Within the other channels,

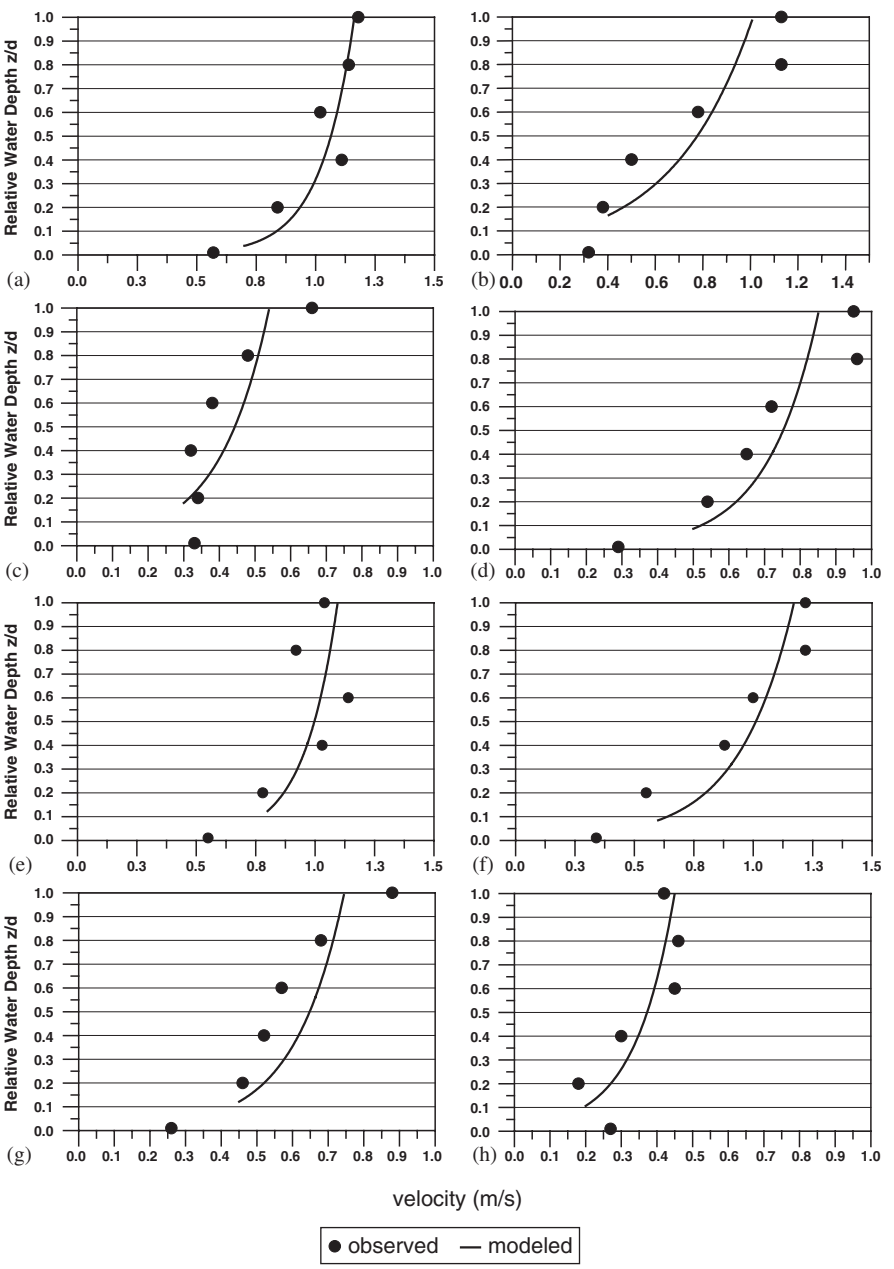

Figure 8. Comparisons of vertical profiles of observed and modelled tidal velocities: (a) 21:00, 12 August 1978; (b) 24:00, 12 August 1978; (c) 02:00, 13 August 1978; (d) 08:00, 12 August 1978 at the Station 16; (e) 17:00, 12 August 1978; (f) 21:00, 12 August 1978; (g) 24:00, 12 August 1978; (h) 08:00, 13 August 1978 at the Station 18.

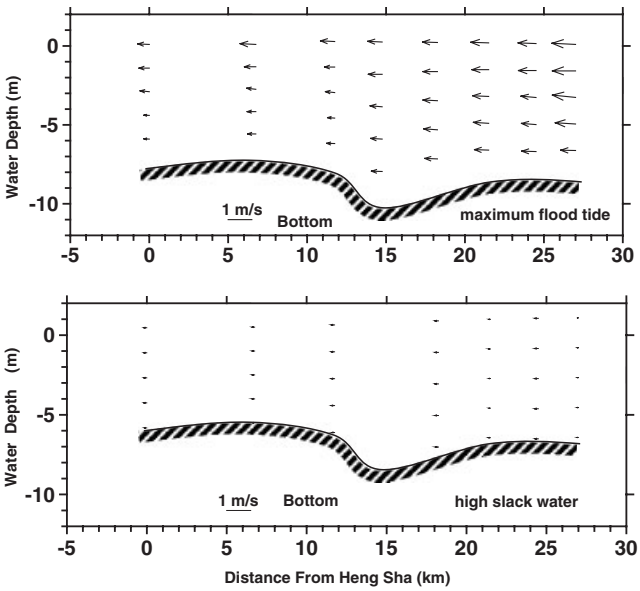

Figure 9. Modelled tidal current velocity field (longitudinal) at maximum flood tide and at high slack water.

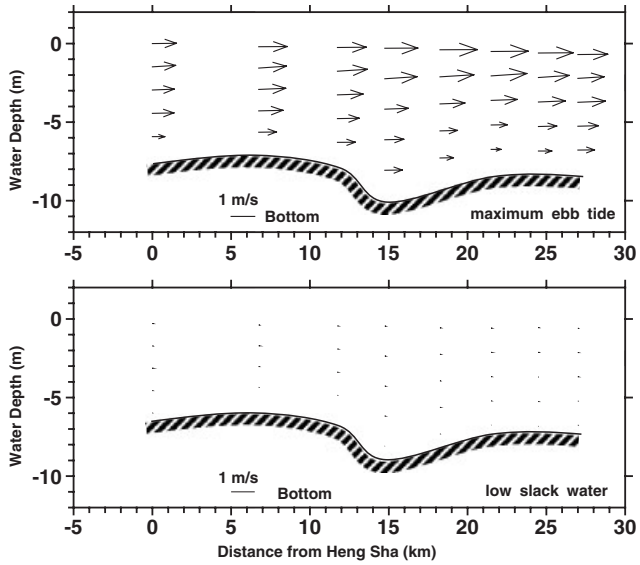

Figure 10. Modelled tidal current velocity field (longitudinal) at maximum ebb tide and at low slack water.

water depths vary between 5.0 and 6.0 m. The set-up represents an idealization of the real Changjiang Estuary as cross-sectional variations, as flood plains, are neglected and that the flow is barotropic.

The model has been verified by hydrographic data (from 1400 h 12 August 1978 to 1200 h 13 August 1978) collected from Stations 16 and 18 (Figure 6) at the North Passage of the Changjiang Estuary. Assuming the estuarine width B is not varied with time, a cross-sectional bottom profile can be schematized as a rectangular bottom profile.

Comparisons of observed and modelled tidal elevations at Stations 16 and 18 are shown in Figures 7(a) and 7(b). They demonstrate a reasonable agreement during all periods of the tidal cycle, i.e. at slack water, early flood tide, maximum flood tide, high slack water, early ebb tide and maximum ebb tide.

Comparisons of observed and modelled velocities at Station 16 are shown in Figures 8(a) –8(d) and at Station 18 in Figures 8(e)–8(h). There is a reasonable agreement between observed and modelled data. However, in Figures 8(b), 8(d) and 8(f), there is an apparent surface layer with increased velocities, indicating the presence of a stratification approximately at a relative depth of 0.7.

In Figures 9 and 10 are shown characteristic longitudinal distributions of modelled tidal velocities through a flood/ebb tidal cycle. The plots are shown for maximum flood tide (Figure 9(a)), high slack water (Figure 9(b)), maximum ebb tide (Figure 10(a)), low slack water (Figure 10(b)).

5. CONCLUSIONS

An efficient 2DV model, coupled with an algebraic turbulence closure sub-model, is established to simulate estuarine tidal flow. In the mean time, a vertically moving finite-element method, without a σ transformation of vertical co-ordinates, is applied to the Changjiang tidal estuary.

The following conclusions can be drawn from this study: (1) σ-co-ordinate transformation is associated with the FDM in the estuarine tidal model; (2) the FEM derivations of the governing equations with σ-co-ordinate transformation become more complicated than without it; and (3) if the governing equations are derived by the FEM, σ-co-ordinate transformation is no longer necessary. The model has been verified with special reference to the Changjiang Estuary.

ACKNOWLEDGEMENTS

This research was supported by the National Science Fund for Distinguished Young Scholars of China (Estuarine and Coastal Studies 40225014) and the Shanghai Rising-Star Program. Dr HJ Zhou is thanked for providing us with the hydrographic data.

REFERENCES

1. Chu WS, Yeh WG. Two-dimensional tidally averaged estuarine model. *Journal of the Hydraulics Division* 1980; **106**(HY4):501–518.
2. Maa JP-Y. An efficient horizontal two-dimensional hydrodynamic model. *Coastal Engineering* 1990; **14**:1–18.
3. Barer RW, Pearson RV, Roberts AP, McKee WI. Numerical simulation of the Humber estuary using a non-orthogonal curvilinear co-ordinate system. In *Computer Modeling of Seas and Coastal Regions II*, Brebbia CA, Traveresoni L, Wrobel LC (eds). Computational Mechanics Publications: Southampton Boston, 1995; 29–37.
4. Mead CT. An investigation of the suitability of two-dimensional mathematical models for predicting sand deposition in dredged trenches across estuaries. *Journal of Hydraulic Research* 1999; **37**(4):447–464.

5. Blumberg AF. Numerical model of estuarine circulation. *Journal of the Hydraulics Division* 1977; **103**(HY3): 295–309.
6. Boericke RR, Hogan JM. An X-Z hydraulic/thermal model for estuaries. *Journal of the Hydraulics Division* 1977; **103**(HY1):19–37.
7. Li ZH, Nguyen KD, Brun-Cottan JC, Martin JM. Numerical simulation of the turbidity maximum transport in the Gironde estuary (France). *Oceanologica Acta* 1994; **17**(5):479–500.
8. Kuo AY, Shen J, Hamrick JM. Effect of acceleration on bottom shear stress in tidal estuaries. *Journal of Waterway, Port, Coastal, and Ocean Engineering* 1996; **122**(2):75–83.
9. Swift MR, Reichard R, Celikkol B. Stress and tidal current in a well-mixed estuary. *Journal of the Hydraulics Division* 1979; **105**(HY7):785–799.
10. Alfrink BK, Van Rijn LC. Two-equation turbulence model for flow in trenches. *Journal of Hydraulic Engineering* 1983; **109**(7):941–957.
11. Grotkop G. Finite element analysis of long period water waves. *Computational Methods in Applied Mechanics and Engineering* 1973; **2**:147–157.
12. Connor JJ, Wang J. Finite element modeling of hydrodynamic circulation. In *Numerical Methods in Fluid Dynamics*, Brebbia CA, Connor JJ (eds). Pentech Press: London, 1974; 355–387.
13. Taylor C, Davis JM. Tidal propagation and dispersion in estuaries. In *Finite Elements in Fluids*, Gallagher RH, Oden JT, Taylor C, Zienkiewics OC (eds). John Wiley: London, 1975; 95–118.
14. Herrling B. Finite element model for estuaries with intertidal flats. *Proceedings of the 15th International Coastal Engineering Conference*, Honolulu, Hawaii, vol. 4. ASCE: New York, U.S.A., 1977; 3396–3415.
15. Smith LH, Cheng RT. Tidal stream flow solved by Galerkin technique. *Proceedings of the 15th International Coastal Engineering Conference*, Honolulu, Hawaii, vol. 4. ASCE: New York, U.S.A., 1977; 3358–3376.
16. Reichard RP, Celikkol B. Application of a finite element hydrodynamic model to the Great Bay estuary system, New Hampshire, U.S.A. In *Hydrodynamics of Estuaries and Fjords*, Nohoul JCJ (ed.). *Proceedings of the 9th International Liege Colloquium on Ocean Hydrodynamics*. Elsevier Oceanography Series, vol. 23. Elsevier: Amsterdam, Oxford, New York, 1978; 349–372.
17. Holz KP. Finite elements, a flexible tool for modeling estuarine processes. In *Mathematical Modeling of Estuarine Physics*, Sundermann J, Holz Kp (eds), Lecture Notes on Coastal and Estuarine Studies. Springer: Berlin, Heidelberg, New York, 1980; 50–61.
18. Li HL, Xia YF. A finite element method for numerical computation of unsteady flow in estuarine branching channels. *Proceedings of International Conference on Coastal and Port Engineering in Developing Countries*, Colombo, 20–26 March 1983; 1340–1354.
19. Li YS, Zhan JM. An efficient three-dimensional semi-implicit finite element scheme for simulation of free surface flows. *International Journal for Numerical Methods in Fluids* 1993; **16**:187–198.
20. Kodama T, Kawahara M. Finite element methods for two-layer tidal current analysis with an open boundary condition. *International Journal of Computational Fluid Dynamics* 1994; **3**:19–51.
21. Malcherek A. Application of TELEMAC-2D in a narrow estuarine tributary. *Hydrological Processes* 2000; **14**:2293–2300.
22. Celik I, Rodi W. Calculation of wave-induced turbulence flows in estuaries. *Ocean Engineering* 1985; **12**(6): 531–542.
23. Lin CP, Mehta AJ. Turbidity-induced sedimentation in closed-up channels. *Journal of Coastal Research* 1989; **5**(3):391–401.
24. Burchard H, Petersen O. Hybridization between σ and z co-ordinates for improving the internal pressure gradient calculation in marine models with steep bottom slopes. *International Journal for Numerical Methods in Fluids* 1997; **25**:1003–1023.
25. Chung TJ. *Finite Element Analysis in Fluid Dynamics*. McGraw-Hill International Book Company: New York, 1978; 1–378.
26. Li SS, Shi Z. 2DV FEM modeling of estuarine tidal flow. *Proceedings of the 29th International Association of Hydraulic Engineering and Research Congress, Theme E, Beijing*, 16–21 *September* 2001; 326–333.
27. Huang S, Lu QM. *Estuarine Dynamics*. Hydraulic Engineering and Hydropower Press: Beijing; 1995; 345–346.
28. Ferziger JH, Peric M. *Computational Methods for Fluid Dynamics.* Springer: Berlin, Heidelberg, Germany, 1996; 321–340.

